PREPARATION AND VISIBLE PHOTOCATALYTIC PROPERTIES OF N-DOPED TiO$_2$/MUSCOVITE NANOCOMPOSITES

Yao Li, Hongjuan Sun*, Tongjiang Peng, Hao You, Li Zeng, and Yating Qin

[1]Key Laboratory of Solid Waste Treatment and Resource Recycle, Southwest University of Science and Technology, Mianyang 621010, China

Abstract—As a photocatalyst with good prospects, TiO$_2$ has the shortcomings of easy agglomeration and no catalytic performance under visible light. The purpose of the present study was to help solve these problems by employing muscovite as a carrier for N-doped TiO$_2$ in a nanocomposite. The nanocomposites were prepared by a liquid precipitation-grinding method using muscovite as the matrix and urea as the nitrogen source. The crystal structures, chemical bonding, and micromorphology of the nanocomposites were analyzed by X-ray diffraction, infrared absorption spectrometry, and field emission scanning electron microscopy, respectively. Visible and ultraviolet (UV-Vis) light absorption of the nanocomposites was analyzed by solid ultraviolet diffuse reflectance spectroscopy. The photocatalytic effect of the nanocomposites was studied based on the degradation of rhodamine B (RhB) solution. The photocatalytic degradation product of RhB was detected by high-performance liquid chromatography-mass spectrometry, revealing that N-doping inhibits the growth of TiO$_2$ nanoparticles. The photocatalytic performance of N-TiO$_2$/muscovite composite nanomaterials decreased with increasing heat-treatment temperature. N-doped TiO$_2$/muscovite nanocomposites that were heated at 400°C showed the best photocatalytic performance under visible-light illumination with an RhB degradation of 97%.

Keywords—Muscovite · N-doping · Photocatalyst · TiO$_2$ · Visible light

INTRODUCTION

As a highly efficient, non-toxic, and highly active photocatalyst, TiO$_2$ has broad application prospects. It has a large forbidden bandwidth (3.28 eV), however, and its photocatalytic response is only in the ultraviolet and not in the visible region. TiO$_2$ powder has the tendency to agglomerate and is difficult to recycle. These shortcomings greatly limit the practical applications of TiO$_2$ powder as a photocatalyst.

An effective method to increase the photocatalytic activity of TiO$_2$ is to dope with different elements, including metals (such as Cu, Fe, Au, and Pt) (Gomes et al., 2017; Obregón et al., 2015) and nonmetals (such as F, B, C, and N) (Asahi et al., 2001; Wang et al., 2012; Yu et al., 2020). Among these elements, N-doping has been considered to be the most promising way to enhance the visible-light response of TiO$_2$ (Jin Wang et al., 2009). A previous study (Sato, 1985) found that N-doped TiO$_2$ exhibits visible-light activity, which presents the first example for modified TiO$_2$ with visible-light activity. N-doped TiO$_2$ was prepared successfully by spraying a gas mixture of N$_2$/Ar into TiO$_2$ (Asahi et al. (2001). Since then, N-doped TiO$_2$ has attracted much research attention (Asahi et al., 2014; Gomes et al., 2019; Huang et al., 2011).

Methods for the preparation of N-doped TiO$_2$ include the sol-gel process, hydrolysis, liquid precipitation, iron implantation, vapor deposition, and templating (Joshi et al., 2012). These techniques use various N sources as precursors. N-doped TiO$_2$ was prepared by Sun et al. (2019) who detected large amounts of NO$_x$ on the TiO$_2$ surface, which were bound via O–Ti–N bonds. Furthermore, Sun et al. (2019) proposed that the amount of N-doping in TiO$_2$ depended greatly on the form of N (e.g. NH$_3$) volatilized from the composite. The effect of N-doping on the morphological structure and photocatalytic activity of TiO$_2$ was studied systematically by Park et al. (2009), revealing that Ti–O–N bonds are formed with TiO$_2$ after N-doping, which endowed TiO$_2$ with visible-light photocatalytic activity. Furthermore, N-doping could inhibit the growth of TiO$_2$ grains and increase the phase transition temperature of anatase to rutile.

Many reports have been published on the microscopic mechanism of the visible-light response of TiO$_2$ induced by N-doping, including orbital hybridization theory, independent energy level theory, and oxygen vacancy theory (Asahi et al., 2014). Among these theories, oxygen vacancy theory is the one most widely recognized. According to this theory, N enters the TiO$_2$ lattice to replace a certain number of the lattice O atoms during the roasting process, leading to visible-light absorption. According to Jansen and Letschert (2000a), O in metal oxide can be replaced by N to form a yellow oxynitride with visible-light response. Huang et al. (2011) prepared an N-modified TiO$_2$ photocatalyst by a modified sol-gel method and studied the degradation of potassium dichromate solution by this modified catalyst under visible-light irradiation. The results showed that urea decomposed to form a sensitizing cyanuramide at 400°C, resulting in a visible-light responsiveness of N-TiO$_2$.

However, N-doping could neither solve the problem of agglomeration nor that of recycling of TiO$_2$. The most popular

---

solution to these problems was to incorporate TiO_2 in a diatomaceous matrix (Chen & Liu, 2016), sericite (Zhou et al., 2012), zeolite (Jansson et al., 2015), montmorillonite (Kun et al., 2006), muscovite (Yao et al., 2019), etc. Most of the existing studies have improved the photocatalytic performance of TiO_2 by a single method. Research on the photocatalytic effect of TiO_2 by employing both ion doping and muscovite loading have not been reported yet.

The objective of the present study was to improve the photocatalytic performance of TiO_2 under visible light by means of incorporating nitrogen-doped TiO_2 into muscovite as a nanocomposite. The hypothesis was that the influence of N substitution and muscovite loading on the photocatalytic performance of such composite materials could be verified through measurements of the structure, morphology, chemical bonding, and light absorption properties of the composite material.

EXPERIMENTAL SECTION

Sample Preparation

The muscovite used was provided by Chenxing Co., Ltd, Shijiazhuang Province, China. Urea was purchased from Chengdu Kelong Co., Ltd., Chengdu Province, China.

The composite $Ti(OH)_4$/muscovite was prepared according to a previously published procedure (Yao et al., 2019), and mixed uniformly with urea at a 1:1 mass ratio. Then, the mixture was calcined in air at a selected temperature (400, 500, 600, or 700°C) for 2 h. The corresponding N-doped TiO_2/muscovite nanocomposite was obtained after cooling to room temperature. The nanocomposites were labeled as N-TM-T, where N-TM stands for N-doped TiO_2/muscovite nanocomposite, and T stands for the calcination temperature. A control was prepared by calcining the starting $Ti(OH)_4$/muscovite composite in air in the absence of urea at 700°C and labeled as TM-700.

Characterization

X-ray diffraction (XRD) patterns were obtained with a PANalytical X'Pert Pro multifunctional powder diffractometer (PANalytical B.V., Eindhoven, The Netherlands) using CuKα radiation at 40 kV and 40 mA, step width of 0.02°2θ, integration time of 1 s, and scanning range from 3 to 80°2θ.

The micromorphology of the samples was observed using a Zeiss Ultra55 field emission scanning electron microscope (Carl Zeiss NTS GmbH, Oberkochen, Germany). The operating voltage was 15 kV, and the energy spectrum was resolved with a resolution larger than 127 eV (MnKα; count rate: 20,000 cps) and the peak shift was <1 eV (MnKα).

The functional groups of the nanocomposites were characterized by Fourier-transform infrared (FTIR) absorption spectrometry (Nicolet-5700 spectrometer; Thermo Fisher Scientific, Waltham, Massachusetts, USA). The samples for FTIR analysis were prepared by the KBr pellet method, and the data collection range was 4000–400 cm^{-1}.

Optical absorption properties of the samples were analyzed using a Shimadzu Solidspec-3700 solid UV-Vis-NIR
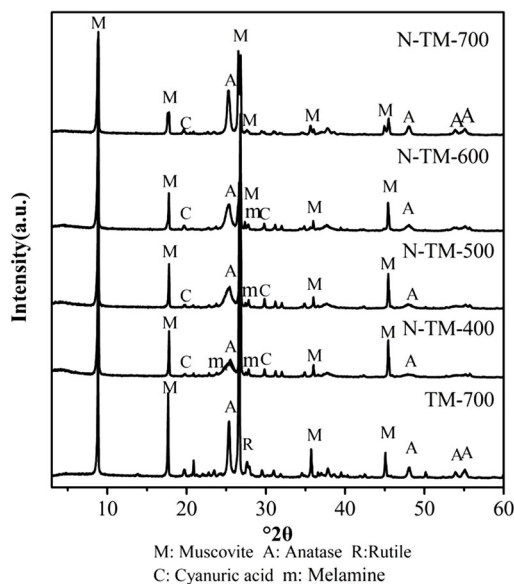

Fig. 1 XRD patterns of N-doped TiO_2/muscovite nanocomposites calcined at various temperatures

spectrophotometer (Shimadzu, Kiya-cho, Nijiyanan, Japan). The resolution was 0.1 nm, the scanning range was between 200 and 800 nm, and $BaSO_4$ was the reference sample.

The intermediate degradation products were identified by high-performance liquid chromatography-mass spectrometry (HPLC-MS, Agilent Technologies, Inc., Santa, Clara, California, USA).

The photocatalytic performances of the nanocomposites were analyzed according to the following procedure. A 500 W xenon lamp (Beijing China Education Au-Light Co., Ltd, Beijing, China) in the visible range of 400–800 nm was used as the illumination source for photocatalytic reactions. A certain amount of photocatalytic material was dispersed in 20 mg/L RhB solution and placed on a magnetic stirrer. The light source was placed 10 cm above the solution. After stirring in the dark for 60 min, the light source was turned on and the supernatant was removed every 20 min. After the reaction, the supernatant was centrifuged to remove catalyst particles. The absorbance of the supernatant was measured on an Evolution 300 UV-Vis spectrophotometer (Shimadzu, Kiya-cho, Nijiyanan, Japan) at the maximum absorption wavelength of

Table 1 Crystallographic data for anatase in the N-TiO_2/muscovite nanocomposite calcined in air at various temperatures

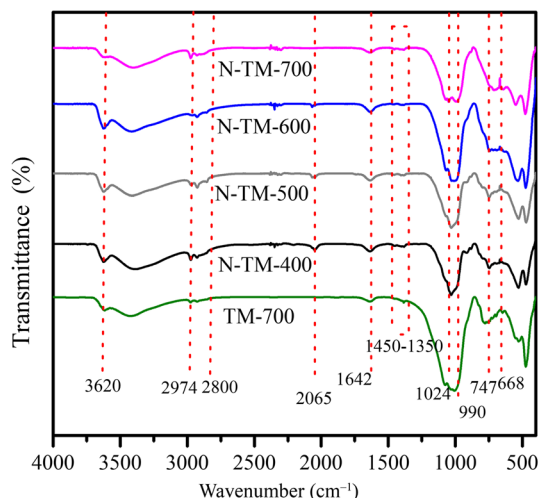| Sample	°2θ$_{(101)}$	$d_{(101)}$ (Å)	FWHM (°2θ)	d_a (nm)
TM-700	25.325	3.52	0.283	9.7
N-TM-400	25.367	3.508	1.259	–
N-TM-500	25.549	3.484	2.954	–
N-TM-600	25.359	3.51	0.883	3.1
N-TM-700	25.268	3.52	0.402	6.8

Fig. 2 FTIR spectra of samples

RhB (554 nm). The concentration change of RhB during the reaction was determined based on the absorbance at the maximum wavelength of the RhB solution, and the degradation rate of RhB was calculated from Eq. 1. The first-order kinetic equation (Eq. 2) was used to fit the photocatalytic data of the samples.

$$D = (A_0 - A_t)/A_0 = (C_0 - C_t)/C_0 \qquad (1)$$

$$-\ln(C_0/C_t) = kt \qquad (2)$$

where A_0 and A_t are the absorbance values of RhB at 554 nm, before and after degradation, respectively, and C_0 and C_t represent the RhB concentrations before and after the degradation, respectively; k is the first-order reaction constant and t represents the reaction time.
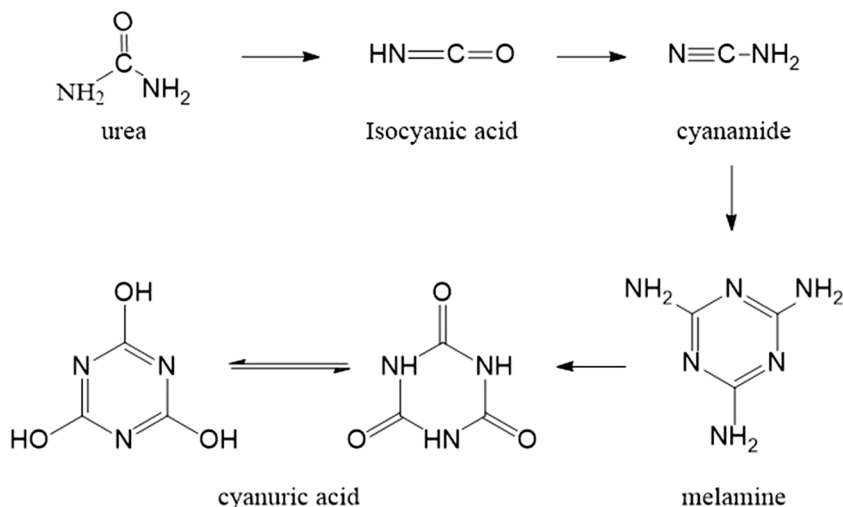
RESULTS AND DISCUSSION

Crystal Structures of N-TiO₂/muscovite Nanocomposites

The XRD patterns of N-TiO₂/muscovite nanocomposites calcined at various temperatures (Fig. 1) revealed that TiO₂ was present in the form of anatase in all the samples. The anatase grain size was calculated by the Scherrer formula (Patterson, 1939), and the results (Table 1) indicated that, compared with the TiO₂/muscovite nanocomposites, the grain sizes of the corresponding N-doped nanocomposites obtained at the same calcination temperature were reduced significantly. N-doping, therefore, inhibits the growth of TiO₂ crystals. No rutile phase was present in any of the samples, indicating that N-doping retards the phase transition of TiO₂ from anatase to rutile. These phenomena were consistent with previous reports (Gomes et al., 2019).

No urea diffraction peaks were detected, indicating complete decomposition of urea. However, the sample calcined at 400°C showed two main diffraction peaks at 26.2 and 29.8°2θ, which were assigned to melamine (Mitoraj & Kisch, 2008) (pdf 00–024–1654). Hauck et al. (2007) reported that melamine was formed by the gradual substitution of the amine group in isocyanic acid by the hydroxyl group. Furthermore, N-TM-500 exhibited a peak at 29.7°2θ, which was assigned to cyanuric acid (Jansen & Letschert, 2000a, 2000b). This indicated that melamine and cyanuric acid were both intermediate products of the decomposition of urea with increasing temperature. Peaks from impurities were assigned to N-containing heterocyclic organic compounds formed as side products in the pyrolysis of urea. One may conclude, therefore, that urea was decomposed and converted into the three intermediates of isocyanic acid: cyanamide, melamine, and cyanuric acid, which were then finally transformed into the N-doped TiO₂/muscovite nanocomposite.

FTIR Analysis

The FTIR spectra of all samples are shown in Fig. 2. The peak at 3620 cm⁻¹ was ascribed to the structural hydroxyl

Fig. 3 Schematic diagram of the chemical process for the urea-decomposition reaction
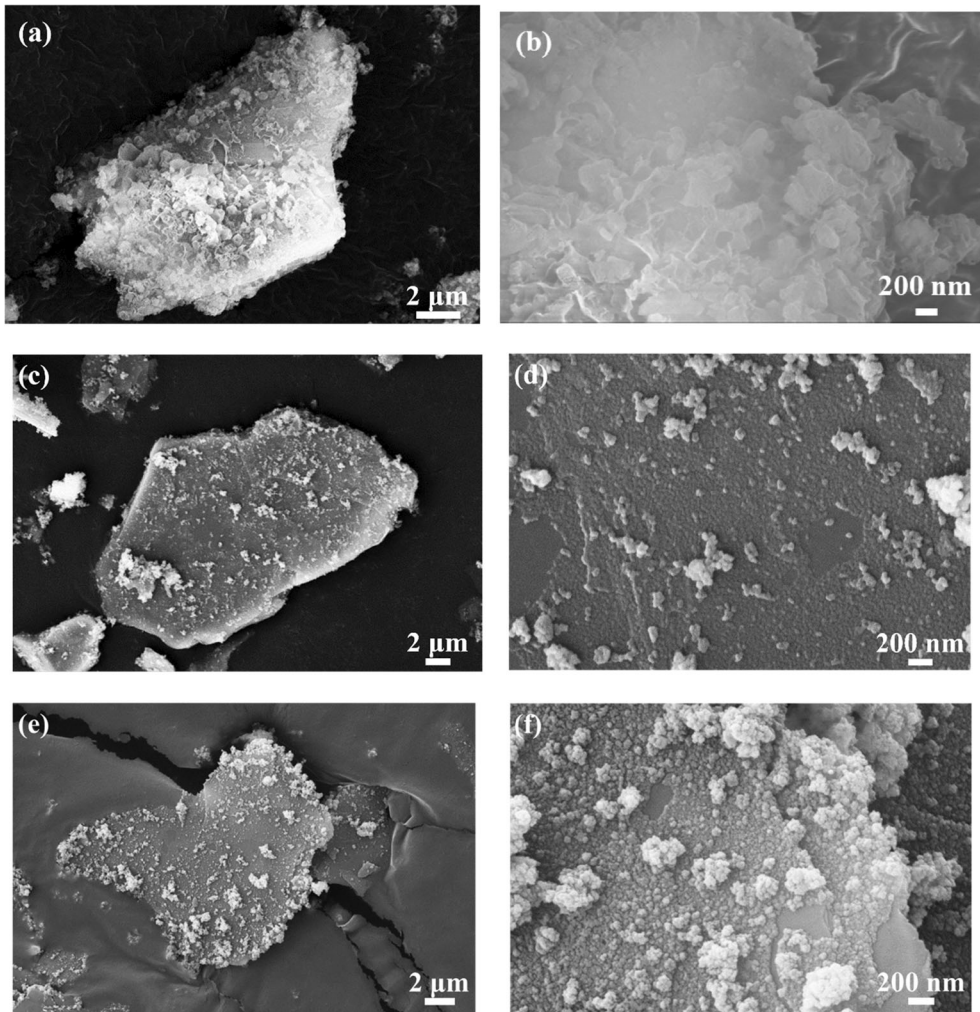
Fig. 4 SEM images of samples **a**, **b** N-TM-400, **c**, **d** N-TM-700, **e**, **f** TM-700

groups of the 2:1 muscovite (Madejová, 2003). This absorption peak decreased with increasing temperature. Absorptions in the region of 3500–3400 cm^{-1} were assigned to the stretching vibration of the O–H bond of adsorbed water. The peak at 1024 cm^{-1} corresponded to the Si–O bond. Peaks in the range of 2974–2800 cm^{-1} corresponded to C–O, which proved the presence of cyanuric acid (Shi et al., 2014). The peak at 2065 cm^{-1} belonged to HNCO (Schaber et al., 2004); its intensity weakened with increasing temperature and disappeared at 700°C. The peak at 1642 cm^{-1} was related to
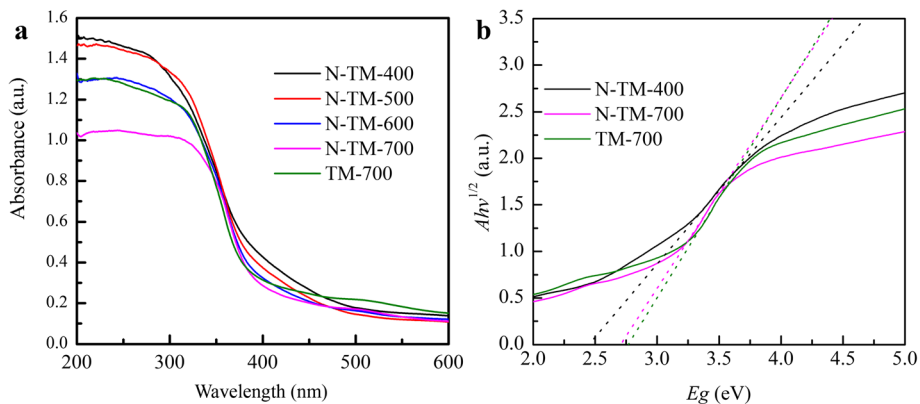

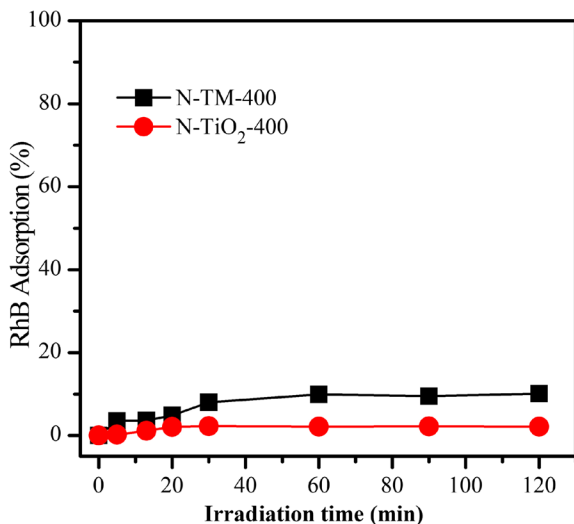**Fig. 5 a** UV-Vis absorption spectra of samples and **b** the Kubelka-Munk function curves

Fig. 6 Adsorption curves of N-TM-400 and N-TiO$_2$-400

Fig. 8 Kinetic fit curves of RhB photocatalytic degradation of various samples

the C=O bond (Schaber et al., 2004) and was overlapped by the absorbance peak related to the flexural vibration of adsorbed water on the surface of the undoped nanocomposite. The peak at 1400 cm^{-1} was attributed to the stretching vibration of the triazine ring (El-Gamel et al., 2008; Huang et al., 2011; Chagas et al., 2012; Jun et al., 2013) of melamine and cyanuric acid. The intensity of this 1400 cm^{-1} peak decreased with increasing temperature, indicating that an increasing number of isocyanic acids decomposed to form N-doped TiO$_2$. A summary of the foregoing analysis of the decomposition of urea is shown by the reaction scheme in Fig. 3.
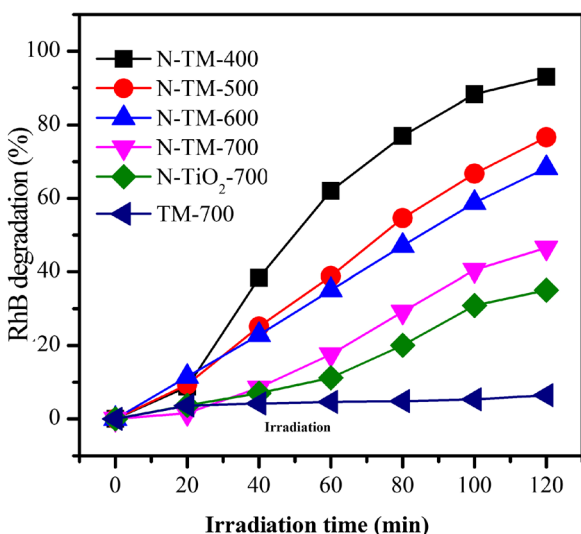

Fig. 7 RhB visible-light photocatalytic degradation rate of the various samples (the pH of RhB solution was 5.15, the concentration of RhB solution was 20 mg/L, the amount of catalyst was 0.05 g in each case)
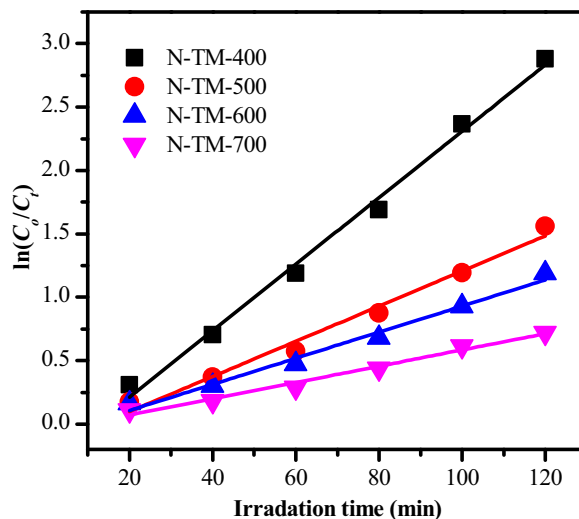
Micromorphology

The SEM images (Fig. 4) of N-TM-400 and N-TM-700 showed that the microscopic morphologies of both nanocomposites were identical to those of the corresponding undoped nanocomposites. The uniformly spherical TiO$_2$ particles formed a coating film on muscovite. In combination with the XRD patterns, the inference is that urea decomposed completely during the calcination process. Furthermore, by comparing Fig. 4d and 4f, the size of TiO$_2$ particles in N-TM-700 was 5 nm, which is smaller than that of TM-700 (10 nm). This indicated that N-doping had a positive effect on the catalyst by inhibiting the growth/agglomeration of TiO$_2$ (Fan et al., 2011). Furthermore, the TiO$_2$ grains in the N-doped nanocomposites were finer and more uniformly distributed than those of the corresponding undoped sample, which improved the photocatalytic ability.

Optical Absorption Characteristics

The UV-Vis absorption spectrum (Fig. 5a) showed that the adsorption of the doped nanocomposites decreased in both UV and visible regions with increasing temperature, which was caused by the formation of larger particles. In addition, the Kubelka-Munk function diagram (Fig. 5b) revealed that the absorbance of the N-doped nanocomposites in both ultraviolet

Table 2 First-order reaction kinetics constants of RhB degradation over various samples

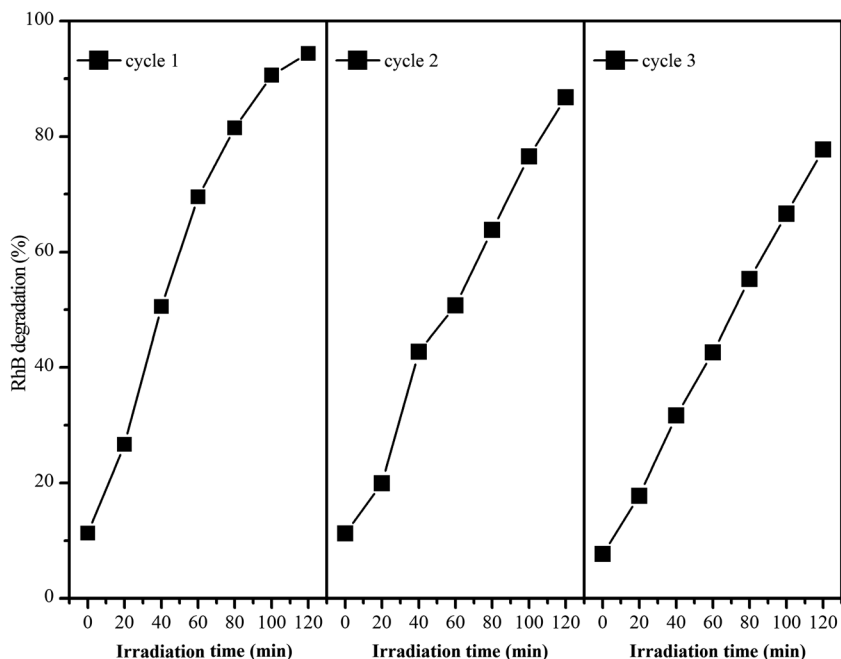| Sample	K (min^{-1})	R^2	First-order kinetic equation
N-TM-400	0.0262	0.992	$y = 0.0262x - 0.312$
N-TM-500	0.0138	0.980	$y = 0.0138\,x - 0.180$
N-TM-600	0.0103	0.983	$y = 0.0103\,x - 0.099$
N-TM-700	0.0064	0.980	$y = 0.0064\,x - 0.057$

Fig. 9 Cyclic photocatalytic degradation of RhB over N-TM-400

and visible regions was improved. N-TM-400 exhibited a forbidden bandwidth (Eg) of 2.45 eV, while the Eg of N-TM-700 was increased to 2.74 eV. The increment of the forbidden bandwidth (Eg) with increasing heat treatment temperature was ascribed to the larger TiO_2 particles (Ekimov et al., 1985). The lower forbidden bandwidth enhanced the visible-light absorption, as well as the visible-light catalytic efficiency, of the nanocomposites. The forbidden bandwidths of the N-doped nanocomposites were smaller than those of the undoped nanocomposites due to the doping of N atoms into TiO_2, which replaced some of the lattice oxygen atoms.

Photocatalytic Degradation Activity

Adsorption ability. The adsorption curves of N-TM-400 and N-TiO_2-400 showed that when the adsorption time was
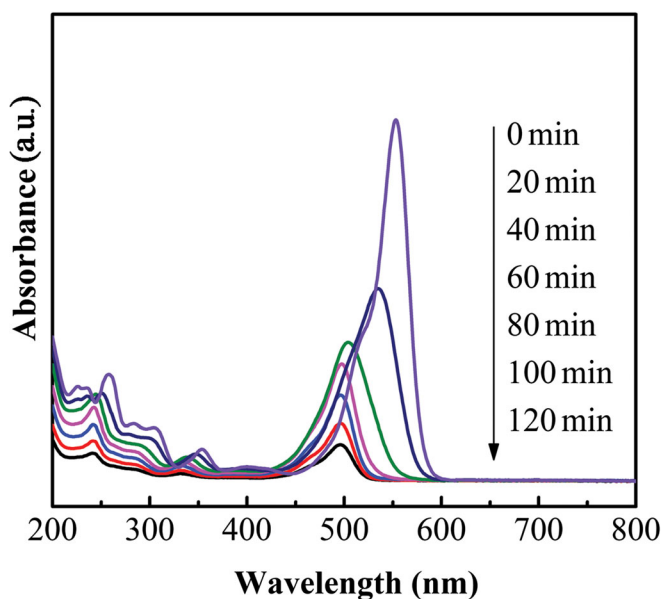

Fig. 10 UV-Vis absorption spectra of RhB degradation by N-TM-400 under visible light
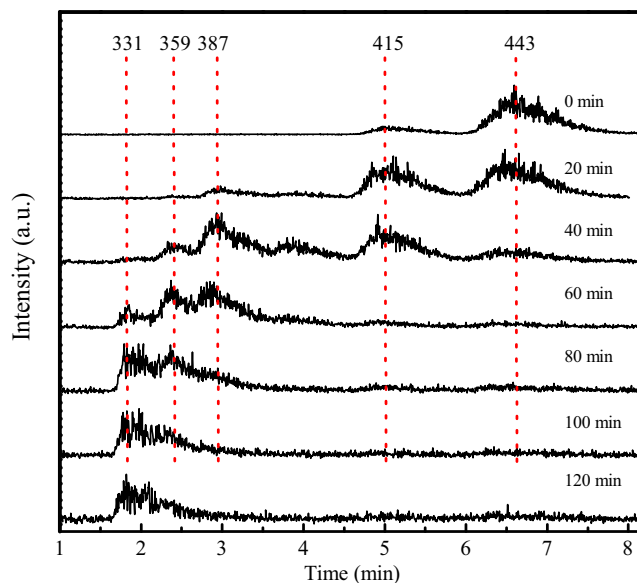
Fig. 11 HPLC-MS of photocatalytic degradation of RhB

>60 min, the adsorption rate remained unchanged (Fig. 6). Therefore, the photocatalytic reaction was started after the solution was stirred for 60 min in the dark. The adsorption of N-TM-400 over that time period was 10.1%. In contrast, N-TiO$_2$ had no adsorption. This indicated that muscovite improved the adsorption ability of catalysts, which was a benefit to the photocatalyst (Laipan et al., 2016).

Effect of heat-treatment temperature on photocatalytic performance. The N-doped TiO$_2$/muscovite nanocomposites had an excellent visible-light photocatalytic ability (Fig. 7)

(Rangel et al., 2018). In contrast, the undoped nanocomposite TM-700 showed no visible-light catalytic effect. The degradation extent of the N-TM-400 after 2 h was 96%, while that of N-TM-700 decreased to 51%. The photocatalytic effect of the N-doped nanocomposites decreased gradually with increasing calcination temperature, which could be ascribed to two effects. On the one hand, the grain size of TiO$_2$ increased with each upward increment of the heat treatment temperature. Therefore, the increasing TiO$_2$ particle agglomeration was accompanied by a decrease in the specific surface area. On the other hand, the greater the calcination temperature, the faster the decomposition of urea and the smaller
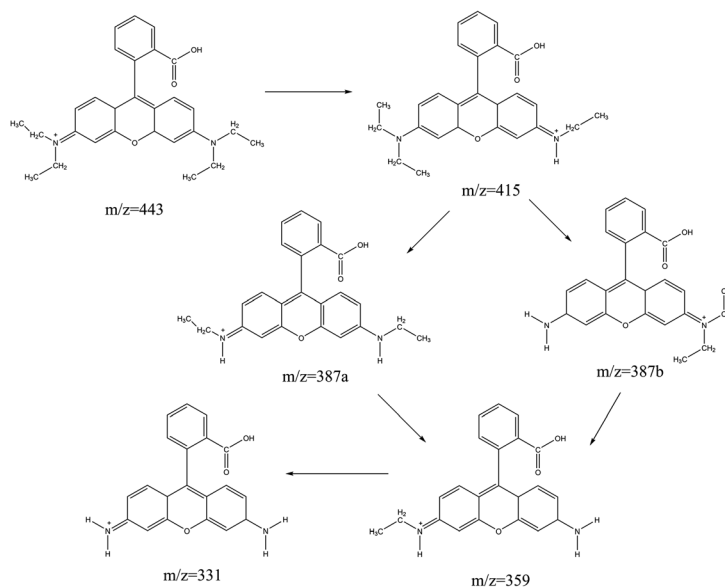

Fig. 12 Schematic diagram of the degradation of RhB

the amount of N-doping in the nanocomposites. As a result, the nanocomposites with lower calcination temperature showed a larger photocatalytic effect.

The photocatalytic degradation of RhB by the N-doped TiO_2/muscovite nanocomposites followed first-order reaction kinetics (Fig. 8 and Table 2), which indicated that the degradation process followed the Eley-Rideal mechanism, and the dissolved pollutant molecules were oxidized and decomposed by the OH generated on the catalyst surface (Liang et al., 2013). In addition, the photocatalysis of N-TM-400 was 0.0262 min^{-1}. Moreover, the N-TiO_2/muscovite composites exhibited a good photocatalytic effect under visible light, which enhances its practical applications.

Cyclic performance. After the photocatalytic reaction, the catalyst was washed ten times alternately with absolute ethanol and deionized water. Then, the catalyst was collected for the photocatalytic cycle experiment. The above steps were repeated three times. The photocatalytic degradation after the third cycle (Fig. 9) was 77%, slightly lower than the first cycle of 94%. This was due to the loss of quality in the catalyst recovery process. Nevertheless, the recyclable performance of the N-doped TiO_2/muscovite nanocomposites was good. In addition, the muscovite loading made the N-TiO_2 photocatalyst easy to be dispersed in and then recovered from the solution, which greatly enhanced its versatility.

Reaction product. The maximum RhB absorption peak of 554 nm exhibited a significant blue shift (to lower wavelength), which was accompanied by a rapid decrease in the peak intensity over time (Fig. 10). This was due to the de-N-ethyl intermediates formed during the degradation of RhB. The main degradation products were identified by HPLC-MS (Fig. 11), revealing that five intermediates were formed in the degradation of RhB during the gradual removal of the N-ethyl group (Fig. 12).

CONCLUSIONS

The N-TiO_2/muscovite nanocomposites were prepared by a liquid precipitation-grinding method using muscovite as the matrix and urea as the nitrogen source. With increasing heat-treatment temperature, urea decomposed gradually into various nitrogen-containing compounds, resulting in N-doping of TiO_2 due to the replacement of O atoms by N atoms. N-doping inhibited the growth/agglomeration of TiO_2 nanoparticles and endowed the nanocomposite materials with a visible-light catalytic effect.

The photocatalytic performance of the N-TiO_2/muscovite composite nanomaterials decreased with increasing heat-treatment temperature. The N-doped TiO_2/muscovite nanocomposites that were treated at a temperature of 400°C showed the best photocatalytic performance with respect to the degradation of RhB, reaching 97% under visible-light irradiation (degradation time: 2 h; 100 mL of 20 mg/L RhB solution).

Photocatalytic degradation by N-doped TiO_2/muscovite nanocomposites followed first-order reaction kinetics. Both N-doping and muscovite loading improved the photocatalytic degradation rate of TiO_2.

Declarations

Conflict of Interest

The authors declare that they have no conflict of interest.

REFERENCES

Asahi, R., Morikawa, T., Irie, H., & Ohwaki, T. (2014). Nitrogen-doped titanium dioxide as visible-light-sensitive photocatalyst: designs, developments, and prospects. *Chemical Review, 114*, 9824–9852.

Asahi, R., Morikawa, T., Ohwaki, T., Aoki, K., & Taga, Y. (2001). Visible-light photocatalysis in nitrogen-doped titanium oxides. *Science, 293*, 269–271.

Chagas, C. A., Pfeifer, R., Rocha, A. B., & Teixeira da Silva, V. (2012). Synthesis of niobium carbonitride by thermal decomposition of guanidine oxaloniobate and its application to the hydrodesulfurization of dibenzothiophene. *Topics in Catalysis, 55*, 910–921.

Chen, Y., & Liu, K. (2016). Preparation and characterization of nitrogen-doped TiO_2/diatomite integrated photocatalytic pellet for the adsorption-degradation of tetracycline hydrochloride using visible light. *Chemical Engineering Journal, 302*, 682–696.

Ekimov, A. I., Efros, A. L., & Onushchenko, A. A. (1985). Quantum size effect in semiconductor microcrystals. *Solid State Communication, 56*, 921–924.

El-Gamel, N. E. A., Wagler, J., & Kroke, E. (2008). Guanidinium cyanurates versus guanidinium cyamelurates: Synthesis, spectroscopic investigation and structural characterization. *Journal of Molecular Structure, 888*, 204–213.

Fan, D., Wu, L., Sun, Y., Min, F., Wu, Z., & Lee, S. C. (2011). Efficient synthesis of polymeric g-C_3N_4 layered materials as novel efficient visible light driven photocatalysts. *Journal of Materials Chemistry, 21*, 15171–15174.

Gomes, J., Lincho, J., Domingues, E., Quinta-Ferreira, R., & Martins, R. (2019). N–TiO_2 photocatalysts: A review of their characteristics and capacity for emerging contaminants removal. *Water, 11*, 373. https://doi.org/10.3390/w11020373.

Gomes, J. F., Leal, I., Bednarczyk, K., Gmurek, M., Stelmachowski, M., Zaleska-Medynska, A., et al. (2017). Detoxification of parabens using UV-A enhanced by noble metals TiO2 supported catalysts. *Journal of Environmental Chemical Engineering, 5*, 3065–3074.

Hauck, P., Jentys, A., & Lercher, J. A. (2007). Surface chemistry and kinetics of the hydrolysis of isocyanic acid on anatase. *Applied Catalysis B: Environmental, 70*, 91–99. https://doi.org/10.1016/j.apcatb.2005.12.025.

Huang, T., Zhang, G., Wang, L., Liu, L., & Sun, X. (2011). Preparation of nitrogen-modified titania with urea as nitrogen source and its modification mechanism. *Chinese Journal of Catalysis (Chinese Version), 32*, 508–512.

Jansen, M., & Letschert, H. P. (2000a). Inorganic yellow-red pigments without toxic metals. *Nature, 404*, 980.

Jansen, M., & Letschert, H. P. (2000b). Inorganic yellow-red pigments without toxic metals. *Nature, 404*, 980–982.

Jansson, I., Suárez, S., Garcia-Garcia, F. J., & Sánchez, B. (2015). Zeolite-TiO₂ hybrid composites for pollutant degradation in gas phase. *Applied Catalysis B: Environmental, 178*, 100–107.

Jin Wang, D. N. T., Lewis, J. P., Hong, Z., Manivannan, A., Zhi, M., Li, M., & Wu, N. (2009). Origin of photocatalytic activity of nitrogen-doped TiO₂ nanobelts. *Journal of the American Chemical Society, 2009*(131), 12290–12297.

Joshi, M. M., Mangrulkar, P. A., Tijare, S. N., Padole, P. S., Parwate, D. V., Labhsetwar, N. K., & Rayalu, S. S. (2012). Visible light induced photoreduction of water by N-doped mesoporous titania. *International Journal of Hydrogen Energy, 37*, 10457–10461.

Jun, Y.-S., Lee, E. Z., Wang, X., Hong, W. H., Stucky, G. D., & Thomas, A. (2013). From melamine-cyanuric acid supramolecular aggregates to carbon nitride hollow spheres. *Advanced Functional Materials, 23*, 3661–3667.

Kun, R., Mogyorosi, K., & Dekany, I. (2006). Synthesis and structural and photocatalytic properties of TiO₂/montmorillonite nanocomposites. *Applied Clay Science, 32*, 99–110.

Laipan, M., Runliang, Z., & Hongping, H. (2016). Visible light assisted Fenton-like degradation of Orange II on Ni₃Fe/Fe₃O₄ magnetic catalyst prepared from spent FeNi layered double hydroxide. *Journal of Molecular Catalysis A: Chemical, 415*, 9–16.

Liang, X. L., He, Z. S., Zhong, Y. H., Tan, W., & Zhang, J. (2013). The effect of transition metal substitution on the catalytic activity of magnetite in heterogeneous Fenton reaction: in interfacial view. *Colloids & Surfaces A: Physicochemical & Engineering Aspects, 435*, 28–35.

Madejová, J. (2003). FTIR techniques in clay mineral studies. *Vibrational Spectroscopy, 31*, 1–10.

Mitoraj, D., & Kisch, H. (2008). The nature of nitrogen-modified titanium dioxide photocatalysts active in visible light. *Angewandte Chemie International Edition, 47*, 9975–9978.

Obregón, S., Muñoz-Batista, M. J., Fernández-García, M., Kubacka, A., & Colón, G. (2015). Cu-TiO₂ systems for the photocatalytic H₂ production: Influence of structural and surface support features. *Applied Catalysis B: Environmental, 179*, 468–478.

Park, Y., Kim, W., Park, H., Tachikawa, T., Majima, T., & Choi, W. (2009). Carbon-doped TiO₂ photocatalyst synthesized without using an external carbon precursor and the visible light activity. *Applied Catalysis B: Environmental, 91*, 355–336.

Patterson, A. L. (1939). The Scherrer formula for X-ray particle size determination. *Physical Review, 56*, 978–982.

Rangel, R., Cedeño, V., Espino, J., Bartolo-Pérez, P., Rodríguez-Gattorno, G., & Alvarado-Gil, J. (2018). Comparing the efficiency of N-doped TiO₂ and N-doped Bi₂MoO₆ photo catalysts for MB and lignin photodegradation. *Catalysts, 8*, 668. https://doi.org/10.3390/catal8120668

Sato, S. (1985). Photocatalytic activity of NOx-doped TiO₂ in the visible light region. *Chemical Physics Letters, 123*, 126–128.

Schaber, P. M., Colson, J., Higgins, S., Thielen, D., Anspach, B., & Brauer, J. (2004). Thermal decomposition (pyrolysis) of urea in an open reaction vessel. *Thermochimica Acta, 424*, 131–142.

Shi, L., Liang, L., Wang, F., Ma, J., & Sun, J. (2014). Polycondensation of guanidine hydrochloride into a graphitic carbon nitride semiconductor with a large surface area as a visible light photocatalyst. *Catalysis Science & Technology, 4*, 207–209.

Sun, Q., Hu, X., Zheng, S., Zhang, J., & Sheng, J. (2019). Effect of calcination on structure and photocatalytic property of N-TiO₂/g-C₃N₄@diatomite hybrid photocatalyst for improving reduction of Cr. *Environmental Pollution, 245*, 53–62.

Wang, P.-P., Huang, B., Dai, Y., & Whangbo, M.-H. (2012). Plasmonic photocatalysts: harvesting visible light with noble metal nanoparticles. *Physical Chemistry Chemical Physics: PCCP, 14*, 9813–9825.

Yao, L., Hongjuan, S., Tongjiang, P., Hao, Y., Yating, Q., & Li, Z. (2019). Effects of muscovite matrix on photocatalytic degradation in TiO₂/muscovite nanocomposites. *Applied Clay Science, 179*, 105155.

Yu, C., Wu, Z., Liu, R., Dionysiou, D. D., Yang, K., Wang, C., & Liu, H. (2020). Corrigendum to "Novel fluorinated Bi₂MoO₆ nanocrystals for efficient photocatalytic removal of water organic pollutants under different light source illumination". *Applied Catalysis B: Environmental*. https://doi.org/10.1016/j.apcatb.2017.02.057

Zhou, S., Lv, J., Guo, L. K., Xu, G. Q., Wang, D. M., Zheng, Z. X., & Wu, Y. C. (2012). Preparation and photocatalytic properties of N-doped nano-TiO₂/muscovite composites. *Applied Surface Science, 258*, 6136–6141.